Robotica: (2020) volume 38, pp. 1463–1477. © Cambridge University Press 2019
doi:10.1017/S0263574719001577

Comparative Kinematic Analysis and Design Optimization of Redundant and Nonredundant Planar Parallel Manipulators Intended for Haptic Use

Houssem Saafi†‡* and Houssein Lamine†

†*Mechanical Laboratory of Sousse (LMS), National Engineering School of Sousse, University of Sousse, Sousse 4000, Tunisia*
E-mail: houssein.lamine@gmail.co
‡*Preparatory Institute for Engineering Studies of Gafsa, University of Gafsa, Gafsa 2000, Tunisia*

(Accepted October 9, 2019. First published online: November 5, 2019)

SUMMARY
This paper investigates a comparative kinematic analysis between nonredundant and redundant 2-Degree Of Freedom parallel manipulators. The nonredundant manipulator is based on the Five-Bar mechanism, and the redundant one is a 3-RRR planar parallel manipulator. This study is aimed to select the best structure for a haptic application. This latter requires a mechanism with a desired workspace of 10 cm × 10 cm and an admissible force of 5 N in all directions. The analysis criteria are the accuracy of the forward kinematic model and the required actuator torques. Thereby, the geometric parameters of the two structures are optimized in order to satisfy the required workspace such that parallel singularities are overcome. The analysis showed that the nonredundant optimally designed manipulator is more suitable for the haptic application.

KEYWORDS: Parallel robot; Singularity; Optimization; Redundancy; Forward kinematic model; Haptic.

1. Introduction

Haptic devices have been developed with the aim to interact with a virtual environment[1,2] or to control a remote robot.[3–5] Generally, these devices sense the users motion and then apply a force feedback. The selection of the kinematic structures and then the design optimization are imperative tasks in order to have transparent devices throughout their workspace (WS) and also to have a uniform distribution of torques.

Parallel manipulators (PMs) are well known for their good accuracy, their stiffness, and their high load capability. These advantages make PMs a good candidate for haptic devices. In fact, based on the parallel structures, several haptic devices have been developed.[4–9] Tobergte et al.[4] designed a 7-Degree Of Freedom (DOF) haptic device based on the Delta structure to control a 7-DOF serial surgical robot. Saafi et al. presented in ref. [5] a new haptic device based on a parallel spherical structure to control a 4-DOF surgical robot. In contrast to the aforementioned spatial devices, regarding planar haptic devices, the most popular architecture is the Five-Bar mechanism.[6–9] Pedemonte et al.[6] proposed a 2-DOF planar haptic device for teaching and improving handwriting. An and Kwon[7] implemented a control approach for a 2-DOF haptic device equipped with DC motors and Magneto Rheological brakes. In ref. [8], Choi et al. presented a novel haptic mouse where the Five-Bar mechanism is employed to generate a 2-DOF force feedback. Tsetserukou et al.[9] developed a wearable haptic display based on the Five-Bar structure that provides haptic sensation at the fingertip.

* Corresponding author. E-mail: houssem.saafi@gmail.com

Although PMs have many advantages, their major limitation is the existence of singularities inside their WS. Two types can be found: serial singularities (SS) and parallel singularities; the latter is the most critical for PMs.[10] Therefore, many works have been carried out to identify and avoid these singularities.[11–14] Gosselin and Angeles[11] studied the singularities of closed-loop mechanisms. Their study showed the presence of three types of singularities. Özdemir[12] studied the PS of the Five-Bar mechanism and their issues related to the inverse dynamic model. Alici[13] developed a systematic approach to obtain singularity contours for a class of the Five-Bar mechanism. Zhou and Ting[14] studied the path generation for the Five-Bar mechanism with singularity avoidance. In this context, for haptic devices, the path is generated by a user during interaction with a virtual environment. Thus, this means that the haptic device may cross PS.

Two solutions may be introduced in aim to eliminate the PS or to cancel their effects. The first solution is the optimization of the geometric parameters to keep the singularities outside the required WS. The second one is the incorporation of redundancy.

On the one hand, the optimization of geometric parameters of PMs is a well-studied problem.[5,15–19] Generally speaking, the optimization goal is conducted to obtain a compact structure that covers a desired WS free from PS. The dexterity index is the most used performance index. It helps to keep singularities outside the desired WS and to get a uniform kinematic performance. Ceccarelli et al.[15] proposed a multiobjective optimization problem for designing both serial manipulator and PM. Lou et al. proposed in ref. [16] a general approach for optimal geometrical design of PMs. The aim of their work is to maximize the singularity-free WS of PMs. Saafi et al.[5] optimized the geometric parameters of a new spherical PM in aim to eliminate PS from a prescribed WS. Rosyid et al.[17] optimized a planar parallel robot for machining applications. Stocco et al. proposed in ref. [18] a new discrete global optimization algorithm to get a globally optimal architecture for a planar haptic interface from both kinematic and dynamic perspectives.

On the other hand, redundancy is introduced to improve the kinematic and dynamic behaviors of PMs.[20–24] There are two types of redundancy: kinematic redundancy and actuator redundancy. For the kinematic redundancy, an extra leg is added to the parallel structure and an extra actuator is placed on the base. For the actuator redundancy, only an extra actuator is placed on a passive joint. The redundancy eliminates the negative effects of PS which can be described as the following. The first effect is the amplification of actuator torques near singular configurations. The second one is the amplification of errors of solving the forward kinematic model (FKM).

Some works had compared the performance of redundant and nonredundant parallel robots.[25,26] The comparison made in ref. [25] showed that the redundant manipulator has better stiffness and payload capability than the nonredundant manipulator. However, the comparison is conducted with the same geometric parameters for the two robots and the intended application is missing. In ref. [27], a comparison between two redundant 3-DOF planar PMs was investigated such that the first has one additional branch and the second has two additional branches. The authors concluded that the former PM has better conditioning index and velocity performance but has smaller stiffness and payload capabilities.

In this paper, the kinematic performance of nonredundant and redundant 2-DOF planar parallel robots is computed and compared. The first manipulator is the Five-Bar mechanism, and the second one is the 3-RRR planar redundant parallel robot. The target application is the development of a 2-DOF planar haptic device having a desired WS of 10 cm × 10 cm and about 5 N applied forces in all directions. It is worth noting that the comparison between the two structures focuses on the accuracy of the FKM and the maximum required actuator torques. Thereby, this work aims to determine the most accurate device with less required torques.

In addition, the geometric parameters of the two structures are optimized in order to keep the required WS free from PS.

This paper is organized as follows. In Section 2, the kinematic models of the Five-Bar mechanism are presented, and the geometric parameters are optimized. The 3-RRR planar redundant PM is studied and optimized in Section 3. Section 4 deals with the comparison between the two structures. Lastly, Section 5 concludes this paper.

2. Kinematics of the Five-Bar Mechanism

This section studies the kinematic models of the Five-Bar mechanism where the geometric parameters are optimized for the intended haptic application. The kinematic description and the geometric

https://doi.org/10.1017/S0263574719001577 Published online by Cambridge University Press

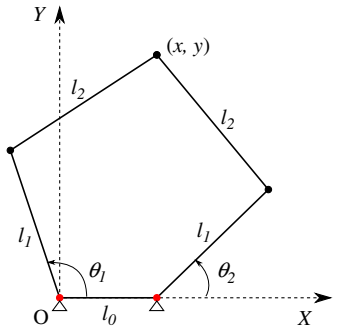

Fig. 1. Notations for the Five-Bar mechanism.

parameters of the Five-Bar mechanism are shown in Fig. 1. This mechanism is composed of two identical branches. Each branch is composed of two links: one connected to the base and the other connected to the end effector. The end-effector position is defined by (x, y) coordinates. l_1 and l_2 are the geometric parameters of the first and second links, respectively. l_0 is the distance between the two actuated joints that are connected to the base. θ_1 and θ_2 are the actuated joint angles. Please note that in the literature various kinematic descriptions and notations were used.[6,7,12,13,28–30]

2.1. Inverse kinematic model

The inverse kinematic model (IKM) gives the active joint angles (θ_1, θ_2) in function of the position of the end effector (x, y). The expression of the active joint angles (θ_1, θ_2) is as follows:

$$\theta_i = 2\ arctan\left(\frac{-B_i \pm \sqrt{A_i^2 + B_i^2 - C_i^2}}{-A_i - C_i}\right) \quad (i = 1, 2) \tag{1}$$

such that:

$$\begin{cases} A_1 = x; \qquad B_1 = y;\ C_1 = \dfrac{l_1^2 - l_2^2 + x^2 + y^2}{2l_1} \\ A_2 = x - l_0;\ B_2 = y;\ C_2 = \dfrac{l_1^2 + l_0^2 - l_2^2 - 2l_0x + x^2 + y^2}{2l_1} \end{cases}$$

Each angle θ_i (for $i = 1, 2$) has two solutions depending on the sign $(\pm)$ in Eq. (1). The combination of the two solutions gives four configurations for the IKM. These different configurations are called working modes (WMs). Figure 2 represents the four WMs for the Five-Bar mechanism. In our case, the WM 1 is selected since there is less interference between the links.

2.2. Jacobian matrix and dexterity

The Jacobian matrix $\mathbf{J}$ defines the relationship between the active joint velocities vector $\dot{\theta}$ and the Cartesian velocity vector $\dot{X}$. This relationship is as follows:

$$\mathbf{J}_x\dot{X} = \mathbf{J}_\theta\dot{\theta} \tag{2}$$

where

$$\dot{X} = \begin{bmatrix} \dot{x} \\ \dot{y} \end{bmatrix}$$

$$\dot{\theta} = \begin{bmatrix} \dot{\theta}_1 \\ \dot{\theta}_2 \end{bmatrix}$$

$$\mathbf{J}_x = \begin{bmatrix} x - l_0/2 - l_1 cos\theta_1 & y - l_1 sin\theta_1 \\ x + l_0/2 - l_1 cos\theta_2 & y - l_1 sin\theta_2 \end{bmatrix}$$

https://doi.org/10.1017/S0263574719001577 Published online by Cambridge University Press

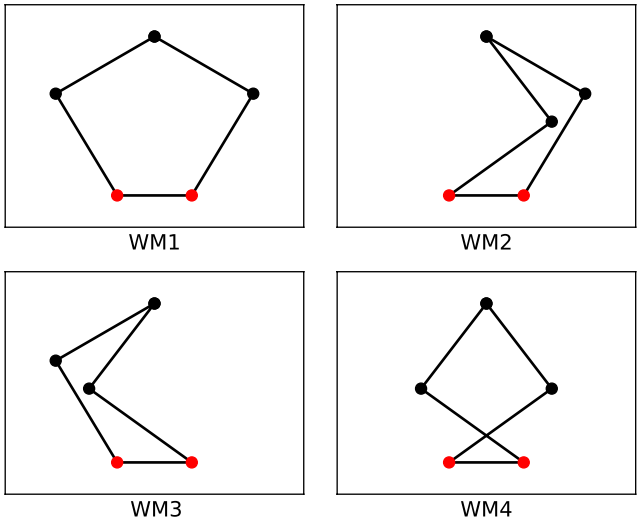

Fig. 2. Working modes of the Five-Bar mechanism.

$$\mathbf{J}_\theta = \begin{bmatrix} l_1 ycos\theta_1 - (x - l_0/2) l_1 sin\theta_1 & 0 \\ 0 & l_1 ycos\theta_2 - (x + l_0/2) l_1 sin\theta_2 \end{bmatrix}$$

The Jacobian matrix of the Five-Bar mechanism is

$$\mathbf{J} = \mathbf{J}_x^{-1} \mathbf{J}_\theta \tag{3}$$

The dexterity index is introduced to measure the kinematic performance of robots. This index gives a measure of how far, the robot is, from a singular configuration. In addition, a good dexterity index ensures a good measure of the robot position via the FKM and also reduces the required joint torques for haptic feedback. The dexterity index expression is defined as:

$$\mu(\mathbf{J}) = \frac{1}{\kappa(\mathbf{J})} \tag{4}$$

with $\kappa(\mathbf{J})$ is the condition number of the Jacobian matrix.

The dexterity distribution for the Five-Bar mechanism is shown in Fig. 3 for the configuration: $l_0 = 100$ mm, $l_1 = 180$ mm and $l_2 = 160$ mm. It shows the presence of PS inside the WS of the robot (shown in dark pink color). To get compact structure with good kinematic performance, the geometrical parameters of the robot should be optimized to keep the PS outside the required WS. The next section deals with the design optimization of the Five-Bar mechanism.

2.3. Design optimization of the Five-Bar mechanism

The useful WS is a (10 cm × 10 cm) square (Fig. 4). The goal of the optimization is to include this square into the robot WS by getting the most compact structure and keeping out the PS.

This square is placed inside the robot WS using the following expressions:

$$\begin{cases} x_0 = l_0/2 \\ y_0 = \dfrac{|l_1 + l_2| - |l_1 - l_2|}{2} + |l_1 - l_2| \end{cases} \tag{5}$$

And the optimization design vector is

$$X = \begin{bmatrix} x_1 \\ x_2 \end{bmatrix} \tag{6}$$

where x_1 and x_2 are the length of the first link and the second link, respectively. The length of the base l_0 is not included in the optimization problem. l_0 is considered to be equal to 100 mm.

https://doi.org/10.1017/S0263574719001577 Published online by Cambridge University Press

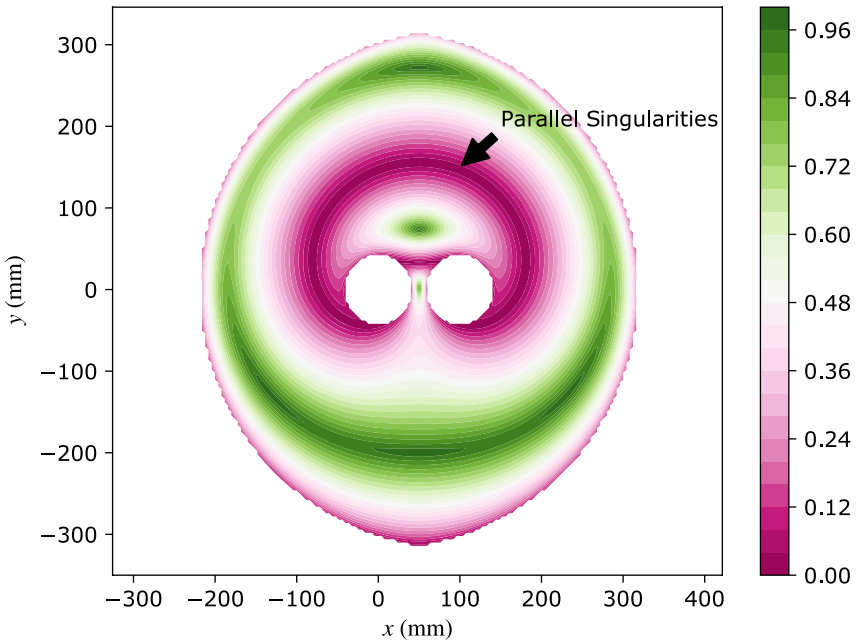

Fig. 3. Dexterity distribution for the Five-Bar mechanism.

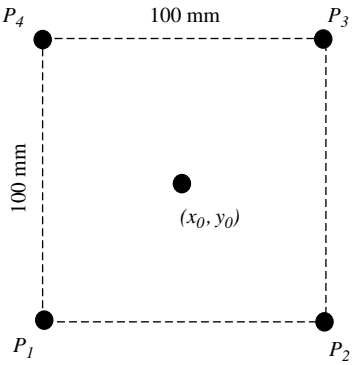

Fig. 4. Useful workspace description.

The optimization problem is formulated as follows:

$$\begin{aligned} \underset{X}{\text{minimize}} \quad & f(X) = x_1^2 + x_2^2 \\ \text{subject to} \quad & P_i \in WS,\ i = 1, \ldots, 4. \\ & \mu(P_i) > 0.5,\ i = 1, \ldots, 4. \end{aligned}$$

The proposed optimization approach is based on the minimization of an objective function $f(X)$ which is the quadratic sum of the robot links (x_1, x_2). The optimization is subject to two constraints. The first constraint involves the WS and aims to guarantee that the haptic device WS fits the prescribed one. The second constraint guarantees the avoidance of PS from the useful WS. Genetic Algorithm is used to minimize the objective function, where the constraints are nonlinear and the lower and upper bounds of x_i are [50, 200] in millimeters. Furthermore, the initial guess is $X_{init} = [90, 150]$ in millimeters.

As a result, the computed optimal design vector is

$$X_{op} = \begin{bmatrix} 85 \\ 142 \end{bmatrix} \text{(in mm)} \tag{7}$$

https://doi.org/10.1017/S0263574719001577 Published online by Cambridge University Press

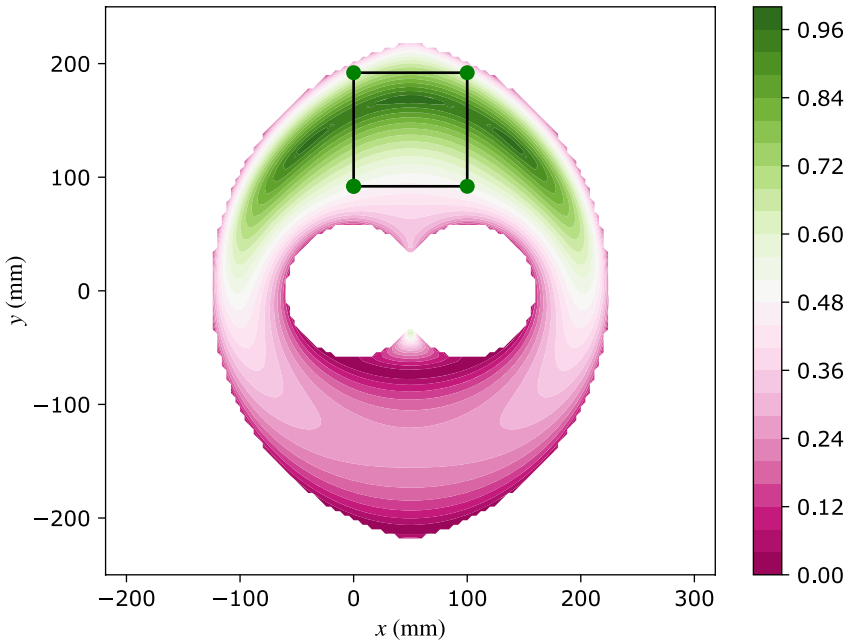

Fig. 5. Optimal dexterity distribution.

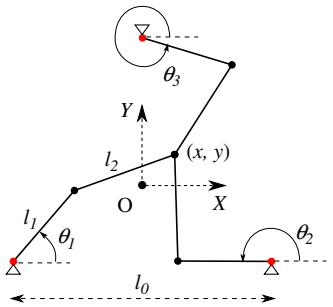

Fig. 6. Geometric parameters of the 3-RRR redundant planar PM.

The dexterity distribution using X_{op} is shown in Fig. 5. One can observe that the dexterity is maximal inside the useful WS with no PS. This optimal structure of the Five-Bar mechanism is used for comparison with the redundant planar robot.

The next section addresses the study and the optimization of the redundant planar parallel robot.

3. Redundant 3-RRR Planar PM

The redundant 3-RRR planar PM is obtained by adding to the Five-Bar mechanism a third branch (Fig. 6). The kinematic modeling of this structure is studied in several works.[25–28] As well as for the Five-Bar mechanism, this redundant parallel robot has 2-DOF. The three active joints are placed on the vertices of an equilateral triangle such that l_0 is the edge length. The base reference frame (O, XY) is placed at the center of the equilateral triangle. l_1 and l_2 are the sizes of the first link and the second link, respectively. The end-effector position is defined by the coordinates (x, y). θ_1, θ_2, and θ_3 are the active joint angles.

3.1. Inverse Kinematic Model

The IKM gives the active joint angles (θ_1, θ_2 and θ_3) in function of the position of the end effector (x, y).

https://doi.org/10.1017/S0263574719001577 Published online by Cambridge University Press

The expression of the active joint angles is as follows:

$$\theta_i = 2\, arctan\left(\frac{-B_i \pm \sqrt{A_i^2 + B_i^2 - C_i^2}}{C_i - A_i}\right) \quad (i = 1, 2, 3) \tag{8}$$

where

$$\begin{cases} A_1 = -2l_1\left(x + \dfrac{l_0}{2}\right);\ B_1 = -2l_1\left(y + \dfrac{\sqrt{3}}{6}l_0\right);\ C_1 = \left(x + \dfrac{l_0}{2}\right)^2 + \left(y + \dfrac{\sqrt{3}}{6}l_0\right)^2 + l_1^2 - l_2^2 \\ A_2 = -2l_1\left(x - \dfrac{l_0}{2}\right);\ B_2 = -2l_1\left(y + \dfrac{\sqrt{3}}{6}l_0\right);\ C_2 = \left(x - \dfrac{l_0}{2}\right)^2 + \left(y + \dfrac{\sqrt{3}}{6}l_0\right)^2 + l_1^2 - l_2^2 \\ A_3 = -2xl_1; \qquad B_3 = -2l_1\left(y - \dfrac{\sqrt{3}}{3}l_0\right);\ C_3 = x^2 + \left(y - \dfrac{\sqrt{3}}{3}l_0\right)^2 + l_1^2 - l_2^2 \end{cases}$$

Each angle θ_i $(i = 1, 2, 3)$ has two solutions depending on the sign $(\pm)$ in Eq. (8). The combination of the two solutions gives eight WMs for the 3-RRR planar PM. For the WM shown in Fig. 6, the sign $\pm$ is $+$ for the three angles.

3.2. Kinematic model of the 3-RRR redundant planar PM

The kinematic model of the 3-RRR redundant planar PM is as follows:

$$\mathbf{J}_x \begin{bmatrix} \dot{x} \\ \dot{y} \end{bmatrix} = \mathbf{J}_\theta \begin{bmatrix} \dot{\theta}_1 \\ \dot{\theta}_2 \\ \dot{\theta}_3 \end{bmatrix} \tag{9}$$

where $\mathbf{J}_x$ is a 3×2 matrix called the parallel part of the Jacobian matrix, and $\mathbf{J}_\theta$ is a 3×3 diagonal matrix called the serial part of the Jacobian matrix.

$$\mathbf{J}_x = \begin{bmatrix} Jx_{11} & Jx_{21} \\ Jx_{12} & Jx_{22} \\ Jx_{13} & Jx_{23} \end{bmatrix} \tag{10}$$

$$\mathbf{J}_\theta = \begin{bmatrix} J_{\theta 11} & 0 & 0 \\ 0 & J_{\theta 22} & 0 \\ 0 & 0 & J_{\theta 33} \end{bmatrix} \tag{11}$$

where $Jx_{1i} = 2l_1 cos\theta_i + A_i/l_1$, $Jx_{2i} = 2l_1 sin\theta_i + B_i/l_1$ and $J_{\theta ii} = B_i cos\theta_i - A_i sin\theta_i$.

Since $\mathbf{J}_\theta$ is a diagonal matrix, the inverse of the Jacobian matrix can be easily expressed as follows:

$$\mathbf{J}^{-1} = \mathbf{J}_\theta^{-1}\mathbf{J}_x \tag{12}$$

The next subsection deals with the optimization of the 3-RRR redundant planar PM.

3.3. Design optimization of the 3-RRR redundant planar PM

Likewise the Five-Bar mechanism, the geometric parameters of the 3-RRR redundant planar PM are optimized using Genetic Algorithm. A similar optimization approach to the one conducted in Section 2.3 is used. In fact, the center of the desired WS (see Fig. 4) is placed at the center of the reference frame (O, XY). The design vector X is composed of the lengths of the first link and the second link, respectively. The optimization problem, which minimizes the sum of the squares of the design vector components, is subject to two constraints: incorporation of the prescribed WS and avoidance of PS. l_0 is considered to be equal to 300 mm, and the lower and upper bounds of x_i are [50; 200] (in mm).

https://doi.org/10.1017/S0263574719001577 Published online by Cambridge University Press

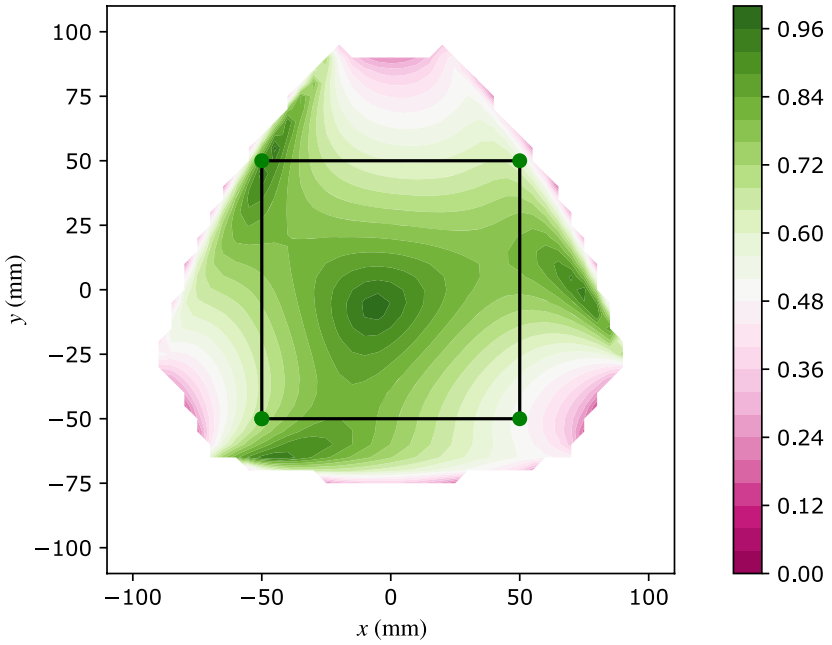

Fig. 7. Optimal dexterity distribution.

Thereby, the obtained optimal design vector is as follows:

$$X_{op} = \begin{bmatrix} 85 \\ 165 \end{bmatrix} \text{(in mm)} \tag{13}$$

The dexterity distribution for the optimal 3-RRR redundant planar PM is shown in Fig. 7. The obtained WS is more compact than the one computed for the Five-Bar mechanism and it is free from PS.

4. Comparison Between the Two Structures

So far, the two addressed manipulators are optimized for the same desired WS. As the intended application is the development of a haptic device, the comparison criteria are the accuracy of the FKM and the maximal required torques for the haptic feedback. In fact, distribution of both the resolution error in terms of positioning and the required torques is plotted. Thereby, the results are compared and discussed.

4.1. FKM accuracy

In this paragraph, the FKM of each structure is established and then the resolution errors are compared.

4.1.1. FKM for the Five-Bar mechanism. The FKM of the Five-Bar mechanism expresses the position of the end effector (x, y) in relation to the active joint angles (θ_1, θ_2):

$$\begin{cases} x = l_1 cos\theta_1 + l_2 cos\gamma_1 = l_0 + l_1 cos\theta_2 + l_2 cos\gamma_2 & (a) \\ y = l_1 sin\theta_1 + l_2 sin\gamma_1 = l_1 sin\theta_2 + l_2 sin\gamma_2 & (b) \end{cases} \tag{14}$$

where γ_1 and γ_2 are the passive joint angles of each leg.

The sum of squares of Eqs. (14a) and (14b) gives

$$A\ sin\gamma_2 + B\ cos\gamma_2 = C \tag{15}$$

https://doi.org/10.1017/S0263574719001577 Published online by Cambridge University Press

where

$$\begin{cases} A = 2l_1l_2sin\theta_2 - 2l_1l_2sin\theta_1 \\ B = 2l_0l_2 - 2l_1l_2cos\theta_1 + 2l_2l_1cos\theta_2 \\ C = l_0^2 + 2l_1^2 - 2l_1^2sin\theta_1 * sin\theta_2 - 2l_1l_0cos\theta_1 \\ \quad +2l_1l_0cos\theta_2 - 2l_1l_1cos\theta_1cos\theta_2 \end{cases}$$

Using the tan-half identities ($t = tan(\gamma/2)$), Eq. (15) is arranged as follows:

$$(B - C)t^2 - 2At - B - C = 0 \tag{16}$$

Thus, the angle γ_2 is expressed as follows:

$$\gamma_2 = 2atan\left(\frac{A + \sqrt{A^2 + B^2 - C^2}}{B - C}\right) \tag{17}$$

Lastly, the position of the end effector (x, y) can be determined using the last part of Eq. (14).

4.1.2. FKM for the 3-RRR planar redundant manipulator. For the 3-RRR planar redundant manipulator, three angles are active. However, the FKM can be expressed only using two active angles as the Five-Bar mechanism. The passive angle γ_2 is determined using the geometric equations of the first leg and the second leg as follows:

$$\begin{cases} x = -\frac{l_0}{2} + l_1cos\theta_1 + l_2cos\gamma_1 = \frac{l_0}{2} + l_1cos\theta_2 + l_2cos\gamma_2 \\ y = -\frac{\sqrt{3}}{6}l_0 + l_1sin\theta_1 + l_2sin\gamma_1 = -\frac{\sqrt{3}}{6}l_0 + l_1sin\theta_2 + l_2sin\gamma_2 \end{cases} \tag{18}$$

where γ_2 is expressed as

$$\gamma_2(1) = 2atan\left(\frac{A_1 + \sqrt{A_1^2 + B_1^2 - C_1^2}}{B_1 - C_1}\right) \tag{19}$$

with

$$\begin{cases} A_1 = -2l_1l_2 * sin\theta_1 + 2l_1l_2sintheta_2 \\ B_1 = 2l_0l_2 - 2l_1l_2cos\theta_1 + 2l_2l_1cos\theta_2 \\ C_1 = l_0^2 + 2l_1^2 + 2l_0l_1(cos\theta_2 - cos\theta_1) \\ \quad -2l_1^2cos(\theta_1 - \theta_2) \end{cases}$$

γ_2 can be determined also using the geometric equations of the second leg and the third leg as follows:

$$\begin{cases} x = \frac{l_0}{2} + l_1cos\theta_2 + l_2cos\gamma_2 = l_1cos\theta_3 + l_2cos\gamma_3 \\ y = -\frac{\sqrt{3}}{6}l_0 + l_1sin\theta_2 + l_2sin\gamma_2 = \frac{\sqrt{3}}{3}l_0 + l_1sin\theta_3 + l_2sin\gamma_3 \end{cases} \tag{20}$$

where γ_2 is expressed as

$$\gamma_2(2) = 2atan\left(\frac{A_2 + \sqrt{A_2^2 + B_2^2 - C_2^2}}{B_2 - C_2}\right) \tag{21}$$

https://doi.org/10.1017/S0263574719001577 Published online by Cambridge University Press

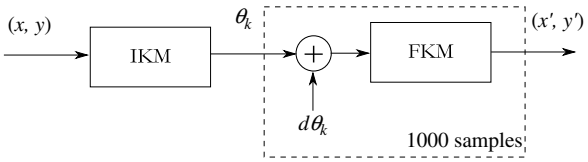

$k = 1, 2$ for the Five-Bar mechanism.
$k = 1, 2, 3$ for the 3-RRR redundant planar manipulator.

Fig. 8. Diagram of the comparison approach.

with

$$\begin{cases} A_2 = -\sqrt{3}l_0l_2 + 2l_1l_2sin\theta_2 - 2l_1l_2sin\theta_3 \\ B_2 = l_0l_2 + 2l_1l_2cos\theta_2 - 2l_1l_2cos\theta_3; \\ C_2 = l_0^2 + 2l_1^2 + \sqrt{3}l_0l_1(sin\theta_3 - sin\theta_2) - 2l_1^2cos(\theta_2 - \theta_3) \\ \qquad +l_1l_0(cos\theta_2 - cos\theta_3) \end{cases}$$

In order to improve the accuracy of the FKM, the final result for the angle γ_2 is the average of the two solutions $\gamma_2(1)$ and $\gamma_2(2)$:

$$\gamma_2 = \frac{\gamma_2(1) + \gamma_2(2)}{2} \tag{22}$$

As well as the Five-Bar mechanism, the position of the end effector (x, y) can be determined using the last part of Eq. (18).

4.1.3. FKM's accuracy comparison. Comparison of the accuracy of the two FKMs is achieved through the determination of the distribution of the resolution errors inside the useful WS using the model shown in Fig. 8.

The useful WS is discretized into a grid of 20×20 points. For each point (x_i, y_j), the IKM is used to determine the active joint angles θ_k; $k = 1, 2$ for the Five-Bar mechanism and $k = 1, 2, 3$ for the 3-RRR redundant PM. Then, the FKM is called 1000 times such that a random value $d\theta_k$ representing the sensors sensitivity is added to the active angles θ_k. $d\theta_k$ is a random value having a normal distribution: the mean value μ is equal to zero and the standard deviation σ is equal to 0.04°.

The error average is calculated using the following expression:

$$\epsilon(x, y) = \frac{\sum_{n=1}^{1000}(\sqrt{(x - x'(n))^2 + (y - y'(n))^2})}{1000} \tag{23}$$

where x' and y' are the vectors composed of 1000 samples returned by the FKMs.

The error distribution inside the useful WS for the Five-Bar mechanism is shown in Fig. 9. It is uniform, and no error amplification can be observed since the WS is free from PS. Indeed, the maximal error is less than 0.2 mm.

On the other hand, the error distribution of the 3-RRR redundant planar PM, shown in Fig. 10, is not uniform. Furthermore, a small amplification can be observed near (x, y)=(50 mm, 50 mm) and (x, y)=(−20 mm, −50 mm). The explanation of this amplification is that the FKM of the redundant robot is solved using two Five-Bar mechanisms: one composed of the first and second legs and the other composed of the second and third legs. These two configurations are shown in Fig. 11. The configurations (x, y)=(50 mm, 50 mm) and (x, y)=(20 mm, 50 mm) are near PS of the Five-Bar mechanisms formed, respectively, by the second and third legs and by the first and second legs. Thus, the use of an extra sensor is not beneficial for the FKM accuracy.

The FKM accuracy study showed that the optimally designed nonredundant manipulator is better than the redundant one. The next subsection compares the two robots for the haptic feedback.

https://doi.org/10.1017/S0263574719001577 Published online by Cambridge University Press

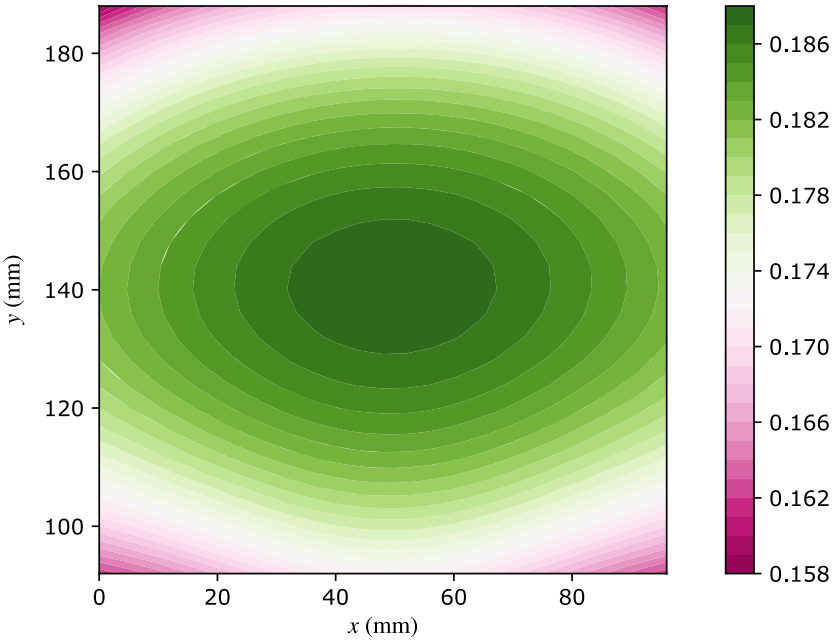

Fig. 9. Error distribution for the Five-Bar mechanism.

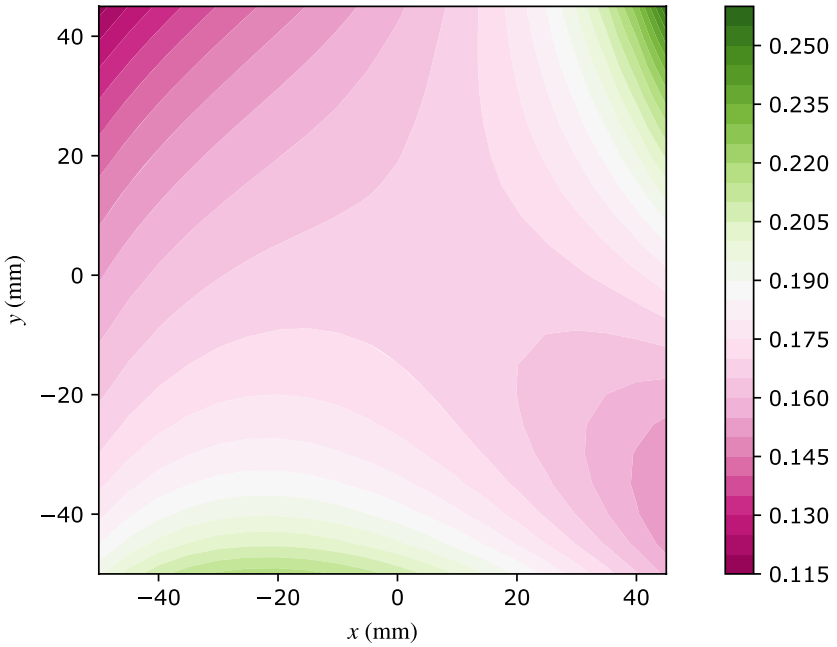

Fig. 10. Error distribution for the 3-RRR redundant planar PM.

4.2. Haptic required torque

4.2.1. Five-Bar mechanism. For the nonredundant PM, the actuator torques vector τ shall produce a given force vector F such that:

$$\tau = \mathbf{J}^T F \tag{24}$$

where $\mathbf{J}$ is the Jacobian matrix.

The gravity effects are neglected because of the horizontal placement of the haptic device. Friction effects are also neglected because of the use of bearings in all robot joints. Thus, the model of Eq. (24) can be used for actuators sizing. In fact, the haptic device is developed to produce a maximal force of 5 N in any direction in the (x,y) plane. To determine the required actuator torques,the useful

https://doi.org/10.1017/S0263574719001577 Published online by Cambridge University Press

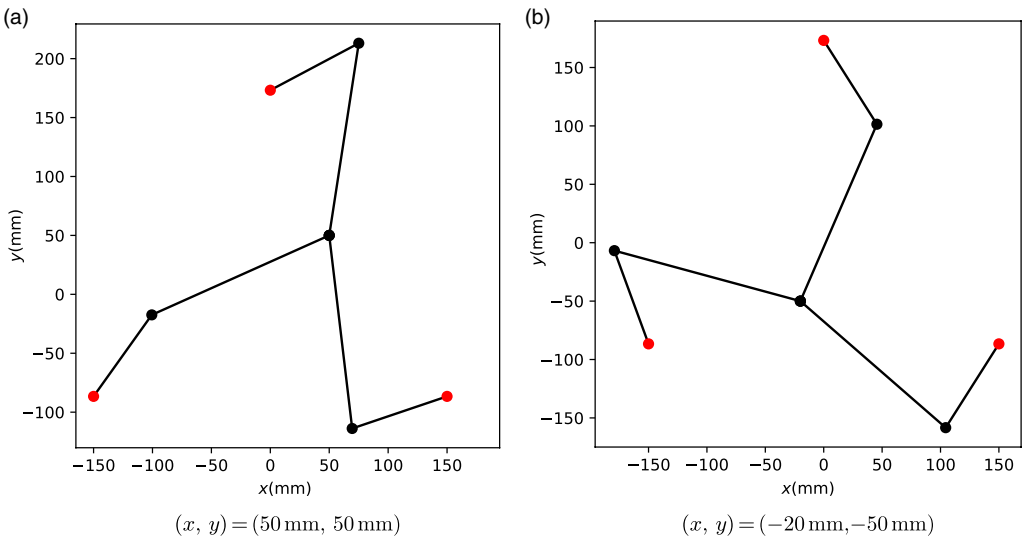

Fig. 11. 3-RRR redundant planar PM configurations.

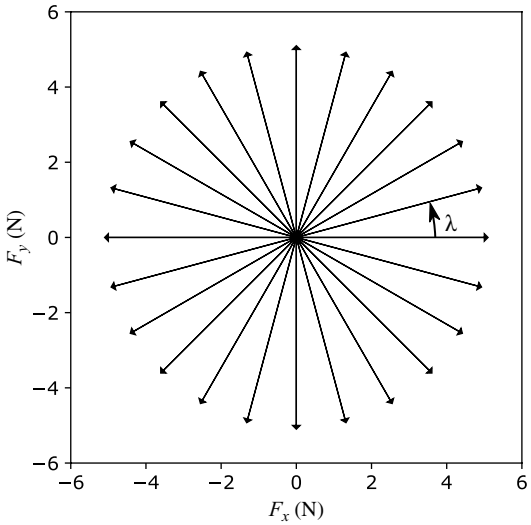

Fig. 12. Force vectors $F(\lambda)$ with $\lambda = 0, \pi/12, \ldots, 2\pi$.

WS is discretized into a grid of 50×50 points. For each point, Eq. (24) is calculated with a force vector $F(\lambda)$ that varies in all directions and is represented in Fig. 12. The expression of $F(\lambda)$ is as follows:

$$F(\lambda) = \begin{bmatrix} 5\ cos(\lambda) \\ 5\ sin(\lambda) \end{bmatrix} \text{(in N)} \quad \lambda = 0, \pi/12, \ldots, 2\pi \tag{25}$$

where λ is an angle defining the orientation of the force vector F. A total of 24 orientations of F are applied for each point.

Figure 13 shows distribution of the maximal torque for each point in the useful WS. The maximal torque value is about 0.45 Nm.

4.2.2. 3-RRR planar redundant manipulator. For redundant PMs, only the force vector can be expressed using the actuator torques vector as follows:

$$F = \mathbf{J}_1^T \tau \tag{26}$$

where $\mathbf{J}_1$ denotes the inverse of the Jacobian matrix.

https://doi.org/10.1017/S0263574719001577 Published online by Cambridge University Press

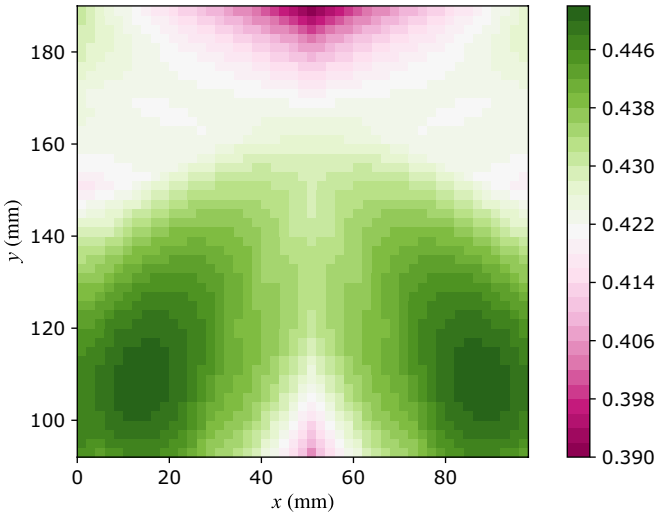

Fig. 13. Maximal torque distribution: $max(\ |\tau(x, y, \lambda)|\ )$.

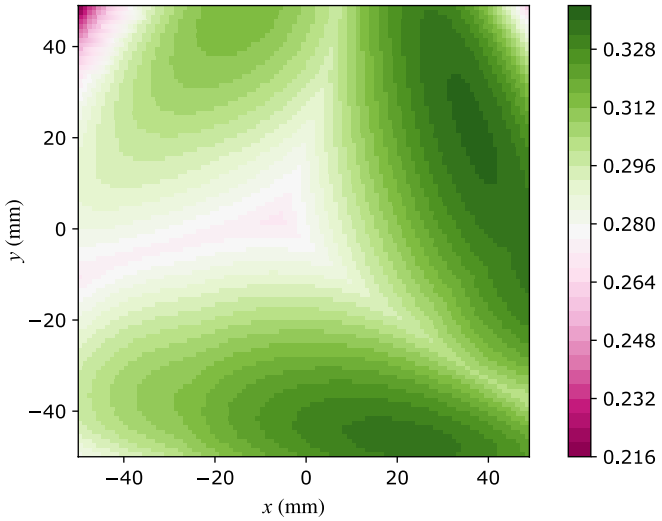

Fig. 14. Maximal torque distribution: $max(\ |\tau(x, y, \lambda)|\ )$.

The pseudo-inverse is used to express the torques vector τ using the force vector F as follows:

$$\tau = (\mathbf{J}_1^T)^+ F + (\mathbf{I} - (\mathbf{J}_1^T)^+ \mathbf{J}_1) Z \tag{27}$$

where $(\mathbf{J}_1^T)^+$ is the pseudo-inverse of $\mathbf{J}_1^T$, $\mathbf{I}$ is the 3×3 unit matrix, and Z is an arbitrary vector. $(\mathbf{I} - (\mathbf{J}_1^T)^+ \mathbf{J}_1) Z$ is the null-space torque which can change the actuator torques τ without affecting the force vector F. To get the optimal torque distribution, the following optimization approach is employed:

$$\underset{Z}{\text{minimize}} \quad f(Z) = \tau_1^2 + \tau_2^2 + \tau_3^2$$

The minimization of $f(Z)$ is performed using a local minimization algorithm, since this function is convex.[31]

Considering actuators sizing, as for the Five-Bar mechanism, the same approach is carried out to determine the maximal actuator torques required for the haptic feedback.

Figure 14 shows the distribution of the maximal torque inside the useful WS. The maximal value is about 0.33 Nm.

https://doi.org/10.1017/S0263574719001577 Published online by Cambridge University Press

4.2.3. Torque distribution comparison. The torque distribution comparison showed that the maximal required torque for the nonredundant parallel robot is higher than for the redundant one. However, the redundant parallel robot requires the use of an extra actuator for the extra leg.

In summary, comparison through the FKM and the required actuator torques showed that the optimally designed PM fits better with the intended haptic application since it has a uniform error distribution for the FKM and in addition it uses less actuators.

5. Conclusions

A comparative analysis between a nonredundant Five-Bar mechanism and a redundant 3-RRR planar manipulator was addressed and investigated. First, the geometric parameters of the two structures were optimized for a desired WS of 10 cm × 10 cm such that PS are avoided. The comparison criteria were the FKM accuracy and the required actuator torques. Regarding the FKM solving, the comparison showed that the optimized nonredundant manipulator has a uniform distribution of errors. Besides, the comparison reported that the required torque per actuator for the redundant manipulator is less than that for the nonredundant one. However, the redundant manipulator requires an extra actuator that rises the actuator's cost when compared with the nonredundant one. Therefore, the optimized and nonredundant manipulator, that is, the Five-Bar mechanism can be selected as a more suitable kinematic structure for the haptic device. Ongoing works are carried out to prototype the haptic device.

References

1. W. Park, L. Kim, H. Cho and S. Park, "Design of Haptic Interface for Brickout Game," *IEEE International Workshop on Haptic Audio visual Environments and Games, HAVE 2009*, Kuala Lumpur, Malaysia (IEEE, 2009) pp. 64–68.
2. F. Gosselin, T. Jouan, J. Brisset and C. Andriot, "Design of a Wearable Haptic Interface for Precise Finger Interactions in Large Virtual Environments," *First Joint Eurohaptics Conference and Symposium on Haptic Interfaces for Virtual Environment and Teleoperator Systems, World Haptics Conference*, Pisa, Italy (IEEE, 2005) pp. 202–207.
3. L. van den Bedem, R. Hendrix, N. Rosielle, M. Steinbuch and H. Nijmeijer, "Design of a Minimally Invasive Surgical Teleoperated Master-Slave System with Haptic Feedback," *International Conference on Mechatronics and Automation, ICMA 2009*, Changchun, China (IEEE, 2009) pp. 60–65.
4. A. Tobergte, P. Helmer, U. Hagn, P. Rouiller, S. Thielmann, S. Grange, A. Albu-Schäffer, F. Conti and G. Hirzinger, "The sigma. 7 Haptic Interface for Mirosurge: A New Bi-Manual Surgical Console," *2011 IEEE/RSJ International Conference on Intelligent Robots and Systems (IROS)*, San Francisco, CA, USA (IEEE, 2011) pp. 3023–3030.
5. H. Saafi, M. A. Laribi, S. Zeghloul and M. Arsicault, "On the development of a new master device used for medical tasks," *J. Mechan. Robot.* **10**(4), 1–6 (2018).
6. N. Pedemonte, T. Laliberté and C. Gosselin, "Bidirectional haptic communication: Application to the teaching and improvement of handwriting capabilities," *Machines* **4**(1), 6 (2016).
7. J. An and D.-S. Kwon, "Five-bar linkage haptic device with DC motors and MR brakes," *J. Intell. Mater. Syst. Struct.* **20**(1), 97–107 (2009).
8. H. Choi, D.-S. Kwon and M.-S. Kim, "Design of Novel Haptic Mouse and its Applications," *2003 IEEE/RSJ International Conference on Intelligent Robots and Systems, IROS 2003*, Las Vegas, NV, USA, vol. 3 (IEEE, 2003) pp. 2260–2265.
9. D. Tsetserukou, S. Hosokawa and K. Terashima, "Linktouch: A Wearable Haptic Device with Five-Bar Linkage Mechanism for Presentation of Two-DOF Force Feedback at the Fingerpad," *Haptics Symposium (HAPTICS)*, Houston, TX, USA (IEEE, 2014) pp. 307–312.
10. J.-P. Merlet and C. Gosselin, "Parallel Mechanisms and Robots," **In:** *Springer Handbook of Robotics* (B. Siciliano and O. Khatib, eds.) (Springer, Berlin, Heidelberg, 2008) pp. 269–285.
11. C. Gosselin and J. Angeles, "Singularity analysis of closed-loop kinematic chains," *IEEE Trans. Robot. Auto.* **6**(3), 281–290 (1990).
12. M. Özdemir, "High-order singularities of 5R planar parallel robots," *Robotica* **37**(2), 233–245 (2019).
13. G. Alıcı, "Determination of singularity contours for five-bar planar parallel manipulators," *Robotica* **18**(5), 569–575 (2000).
14. H. Zhou and K.-L. Ting, "Path generation with singularity avoidance for five-bar slider-crank parallel manipulators," *Mechan. Mach. Theory* **40**(3), 371–384 (2005).
15. M. Ceccarelli, G. Carbone and E. Ottaviano, "An Optimization Problem Approach for Designing Both Serial and Parallel Manipulators," *Proceedings of MUSME 2005, the International Symposiom on Multibody Systems and Mechatronics*, Uberlandia, Brazil (2005) pp. 6–9.
16. Y. Lou, G. Liu, J. Xu and Z. Li. "A General Approach for Optimal Kinematic Design of Parallel Manipulators," *IEEE International Conference on Robotics and Automation, ICRA'04 2004*, New Orleans, LA, USA, vol. 4 (2004) pp. 3659–3664.

17. A. Rosyid, B. El-Khasawneh and A. Alazzam, "Genetic and hybrid algorithms for optimization of non-singular 3PRR planar parallel kinematics mechanism for machining application," *Robotica* **36**(6), 839–864 (2018).
18. L. Stocco, S. E. Salcudean and F. Sassani, "Fast constrained global minimax optimization of robot parameters," *Robotica* **16**(6), 595–605 (1998).
19. R. Unal, G. Kiziltas and V. Patoglu, "A Multi-criteria Design Optimization Framework for Haptic Interfaces," *2008 Symposium on Haptic Interfaces for Virtual Environment and Teleoperator Systems*, Waltham, MA, USA (2008) pp. 231–238.
20. H.-S. Shim, T. Seo and J. W. Lee, "Optimal torque distribution method for a redundantly actuated 3-rrr parallel robot using a geometrical approach," *Robotica* **31**(4), 549–554 (2013).
21. J. H. Choi, T. Seo and J. W. Lee, "Torque distribution optimization of redundantly actuated planar parallel mechanisms based on a null-space solution," *Robotica* **32**(7), 1125–1134 (2014).
22. H. Saafi, M. A. Laribi and S. Zeghloul, "Redundantly actuated 3-RRR spherical parallel manipulator used as a haptic device: Improving dexterity and eliminating singularity," *Robotica* **33**(5), 1113–1130 (2015).
23. A. G. Ruiz, J. C. Santos, J. Croes, W. Desmet and M. M. da Silva, "On redundancy resolution and energy consumption of kinematically redundant planar parallel manipulators," *Robotica* **36**(6), 809–821 (2018).
24. J. H. Lee, B.-J. Yi, S.-R. Oh and I. H. Suh, "Optimal Design of a Five-Bar Finger with Redundant Actuation," *1998 IEEE International Conference on Robotics and Automation, 1998*, Leuven, Belgium, vol. 3 (IEEE, 1998) pp. 2068–2074.
25. J. Wu, J. Wang and L. Wang, "A comparison study of two planar 2-DOF parallel mechanisms: One with 2-RRR and the other with 3-RRR structures," *Robotica* **28**(6), 937–942 (2010).
26. W. Shang and S. Cong, "Dexterity and adaptive control of planar parallel manipulators with and without redundant actuation," *J. Comput. Nonlinear Dyn.* **10**(1), 011002 (2015).
27. J. Wu, T. Li, J. Wang and L. Wang, "Performance analysis and comparison of planar 3-dof parallel manipulators with one and two additional branches," *J. Intell. Robot. Syst.* **72**(1), 73–82 (2013).
28. A. A. Salem, T. Y. Khedr, G. El Ghazaly and M.I. Mahmoud, "Modeling and Performance Analysis of Planar Parallel Manipulators," *International Conference on Advanced Intelligent Systems and Informatics*, Cairo, Egypt (Springer, 2017) pp. 13–23.
29. L. Campos, F. Bourbonnais, I. A. Bonev and P. Bigras, "Development of a Five-Bar Parallel Robot with Large Workspace," *ASME 2010 International Design Engineering Technical Conferences and Computers and Information in Engineering Conference*, Montreal, Quebec, Canada (American Society of Mechanical Engineers, 2010) pp. 917–922.
30. M. G. Villarreal-Cervantes, C. A. Cruz-Villar, J. Alvarez-Gallegos and E. A. Portilla-Flores, "Differential evolution techniques for the structure-control design of a five-bar parallel robot," *Eng. Opt.* **42**(6), 535–565 (2010).
31. H. Saafi, M. A. Laribi and S. Zeghloul, "Optimal torque distribution for a redundant 3-RRR spherical parallel manipulator used as a haptic medical device," *Robot. Auto. Syst.* **89**, 40–50 (2017).

https://doi.org/10.1017/S0263574719001577 Published online by Cambridge University Press